On moments and scaling regimes in anomalous random walks

Michael Schmiedeberg[1]**, Vasily Yu Zaburdaev**[2] **and Holger Stark**[2]

[1] Department of Physics and Astronomy, University of Pennsylvania, 209 South 33rd Street, Philadelphia, PA 19104, USA
[2] Institut für Theoretische Physik, Technische Universität Berlin, Hardenbergstrasse 36, D-10623 Berlin, Germany
E-mail: mschm@sas.upenn.edu, vasily.zaburdaev@tu-berlin.de and holger.stark@tu-berlin.de

Abstract. More and more stochastic transport phenomena in various real-world systems prove to belong to the class of anomalous diffusion. This paper is devoted to the scaling of diffusion—a very fundamental feature of this transport process. Our aim is to provide a comprehensive theoretical overview of scaling properties, but also to connect it to the analysis of experimental data.

Anomalous diffusion is commonly characterized by an exponent in the power law of the mean square displacement as a function of time $\langle \mathbf{r}^2(t) \rangle \propto t^{2\nu}$. On the other hand, it is known that the probability distribution function of diffusing particles can be approximated by $(1/t^\alpha)\Phi(\mathbf{r}/t^\alpha)$. While for classical normal diffusion this scaling relation is exact, it may not be valid globally for anomalous diffusion. In general, the exponent α obtained from the scaling of the central part of the probability distribution function differs from the exponent ν given by the mean square displacement. In this paper we systematically study how the scaling of different moments and parts of the probability distribution function can be determined and characterized even when no global scaling exists. We consider three rigorous methods for finding, respectively, the mean square displacement exponent ν, the scaling exponent α and the profile of the scaling function Φ. We also show that alternatively the scaling exponent α can be determined by analyzing fractional moments $\langle |\mathbf{r}|^q \rangle$ with $q \ll 1$. All analytical results are obtained in the framework of continuous-time random walks. For a wide class of coupled random walks, including the famous Lévy walk model, we introduce a new unifying description which allows straightforward generalizations to other

systems. Finally, we show how fractional moments help to analyze experimental or simulation data consistently.

Keywords: transport properties (theory), dynamics (theory), diffusion

Contents

1. Introduction

Anomalous diffusion occurs in various systems. To name a few, these are particles in external fields [1], turbulent flows [2]–[4] or billiard systems [5]–[8], as well as cells, animals in biological systems [9]–[13] and even human beings [14, 15] may diffuse anomalously. Usually, in theory anomalous dynamics is described by continuous-time random walks (CTRWs) [2]–[4], [8, 10], [16]–[28], [30]. In general, such a random walk is given by a random sequence of steps and intermediate waiting times that are characterized by respective distribution functions for the step length and waiting time.

The purpose of this paper is to study the properties of anomalous diffusion when the probability distribution function (PDF) for the particle position does not exhibit global scaling. Already in the random walk of a particle with finite constant velocity v the tails of the PDF do not show normal diffusive scaling. Instead, they are cut off at the 'light front' $x = vt$, which moves ballistically. For a wide class of random walks, we introduce in this paper a new universal framework that allows us to analytically treat all models in a common way. We systematically analyze how different parts of the PDF and its moments scale and clarify, for the first time, to what extent these results represent valid approximations. As a consequence of our results, we propose how experimental

data should be analyzed. In particular, we show that, in contrast to the mean square displacement (MSD), the moments $\langle |\mathbf{r}|^q \rangle$ with small q are always related to the scaling behavior of the PDF. Furthermore, we demonstrate that, in the case of poor statistics of experimental or simulation data, these moments can usually be determined with a better accuracy than the MSD.

In practice, there are different ways to characterize anomalous diffusion. Especially in the analysis of experimental data, usually the exponent ν given by the relation

$$\langle r^2(t) \rangle \propto t^{2\nu} \tag{1}$$

is determined, where $\langle r^2(t) \rangle = \langle |\mathbf{r}(t) - \mathbf{r}(0)|^2 \rangle$ is the MSD as a function of time. Averaging is performed over all trajectories of diffusing particles. The case $\nu = 1/2$ corresponds to normal diffusion, whereas systems with $\nu > 1/2$ are called superdiffusive and $\nu < 1/2$ denotes subdiffusive behavior. However, as we will explain in this paper in more detail, ν gives very limited information about the transport process. For example, ν not necessarily gives the correct scaling of the PDF (see below). Furthermore, sometimes the MSD diverges (for so-called Lévy flights) and therefore a characterization according to (1) is impossible. In this case one may try to analyze the behavior of the mean absolute value of displacement or even its fractional power. As we will show, scaling exponents obtained in this way have to be interpreted very carefully. Another experimentally accessible quantity is the PDF $P(\mathbf{r}, t)$, which is the probability density to find a particle at time t in a region between $\mathbf{r}$ and $\mathbf{r} + \mathrm{d}\mathbf{r}$. Anomalous diffusion can also be characterized by the scaling of the PDF. A distribution $P(\mathbf{r}, t)$ describing a normal or anomalous diffusive process scales 'perfectly' or globally if there exists a function $\Phi(\mathbf{r})$ and an exponent α such that

$$P(\mathbf{r}, t) = \frac{1}{t^\alpha} \Phi\left(\frac{\mathbf{r}}{t^\alpha}\right) \tag{2}$$

for all positions $\mathbf{r}$ and all times t. The prefactor $1/t^\alpha$ follows from the normalization condition for $P(\mathbf{r}, t)$. In systems with perfect scaling of the PDF, e.g. in the case of classical normal diffusion where $P(\mathbf{r}, t)$ is a Gaussian, the exponent ν defined in (1) equals the scaling exponent α. Lévy-stable distributions also fall into this category. However, there are many systems where perfect scale invariance is broken and only the central part of the distribution $P(\mathbf{r}, t)$ scales according to (2). Then, in general $\alpha \neq \nu$.

In addition to the scaling exponent α, it is possible to determine the shape of the scaling function $\Phi(\xi)$ which then gives the most complete description of the diffusion process.

Finally, another approach to scaling considers general moments $\langle |\mathbf{r}(t)|^q \rangle = \langle |\mathbf{r}(t) - \mathbf{r}(0)|^q \rangle$ as a function of time. The exponent $\nu(q)$ in the relation (see, e.g., [24, 31])

$$\langle |\mathbf{r}(t)|^q \rangle \propto t^{q\nu(q)} \tag{3}$$

depends on the real exponent q. In the case of non-constant $\nu(q)$, the diffusion is sometimes called strongly anomalous [31]. We show for a class of coupled random walks that for $q \ll 1$ $\nu(q)$ approaches the exponent α given by (2) for the scaling of the central part of $P(\mathbf{r}, t)$. Therefore, in general one has four quantities to characterize anomalous diffusion: the scaling exponent of the MSD if it exists, the scaling exponent of the PDF, its asymptotic profile represented by Φ in (2) and the scaling exponents of the fractional moments. Hence, for a complete characterization of anomalous diffusion they

give complementary information. For the first time, models of coupled random walks are presented in a universal framework and three analytical methods are summarized and compared in order to study their asymptotic behavior. All results are supported by computer simulations. This work presents rigorous analytical results which we believe are important and needed for any specialist working with anomalous diffusion. Some of the results were already available in the literature, but only together with our new contributions do they give a unifying and comprehensive picture.

The outline of this paper is the following: in section 2, we introduce the models that we use throughout this paper as examples. We calculate their exponents ν defined by the MSD in section 3 before we determine the scaling exponents α of their PDFs in section 4. In section 5 we explain how the asymptotic profile of the PDF can be found. The exponents $\nu(q)$ for fractional moments are analyzed in section 6. In section 7 we explain how experimental data can be analyzed systematically to correctly characterize the scaling properties of a system. Finally, we conclude in section 8.

2. Examples

Different CTRWs are often treated by similar analytical approaches. As a simple example, we consider here the standard CTRW model where step length and waiting time distributions are independent of each other. However, in many systems random motion occurs with a certain velocity and therefore the time of a step is coupled to the length through this velocity. To cover these cases, we consider also three coupled models, which describe normal diffusive, superdiffusive or ballistic motion. We demonstrate that all these models can be analyzed within one universal formalism. Furthermore, our calculations can easily be applied to other CTRW models, e.g. to random walks with more advanced couplings [21, 28] or with random velocities [23, 29, 30].

A random walker starts in $\mathbf{r} = \mathbf{0}$ at time $t = 0$, i.e. $P(\mathbf{r}, 0) = \delta(\mathbf{r})$. To describe the probability $f(t)$ for a step with a duration in $[t, t + \mathrm{d}t]$, usually a power law distribution

$$f(t) = \frac{\mu}{(1+t)^{\mu+1}} \tag{4}$$

with $\mu > 0$ is considered. It is observed in real systems and is mathematically convenient. In the standard CTRW (see, e.g., [24, 17]) the step length is also given by a power law distribution

$$g_s(\mathbf{r}) \propto \frac{1}{(1+|\mathbf{r}|)^{\beta+1}} \tag{5}$$

with $\beta > 0$. In the standard model step length and duration are decoupled, i.e. they do not depend on each other. In contrast, we also introduce three models where the length of the steps is coupled to the step duration by a constant velocity v, i.e. for a step with duration t one finds a step of length $|\mathbf{r}| = vt$. Such a coupling is suitable for describing many real systems because it is normal to assume that long steps also require a longer time. Moreover, the finite velocity of the motion of the particle is often inherent to the system in question. All directions of $\mathbf{r}$ occur with the same probabilities. Therefore, the probability distribution $g(|\mathbf{r}|)$ for a step of length $|\mathbf{r}|$ is

$$g(|\mathbf{r}|) = \int \mathrm{d}t'\, \delta(t' - |\mathbf{r}|/v) f(t') = \frac{f(|\mathbf{r}|/v)}{\int \mathrm{d}\mathbf{r}'\, f(|\mathbf{r}'|/v)}. \tag{6}$$
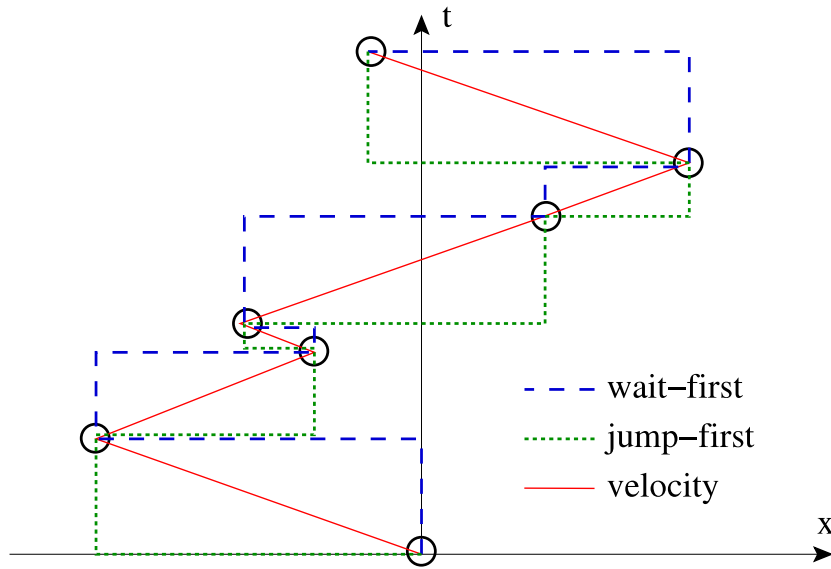
Figure 1. Schematic representation of a path for the coupled models in one dimension plotted in a position–time diagram. The start and end points of a step are the same in all models (marked by circles): however, the paths in between differ from each other: dashed line for the wait-first, dotted line for the jump-first and solid line for the velocity model.

In one dimension, for example, $g(|\mathbf{r}|) = f(|\mathbf{r}|/v)/(2v)$. In particular, we consider the following coupled models (see also figure 1):

- Wait-first model: the random walker first waits for the duration t of a step and then jumps instantaneously along the vector $\mathbf{r}$ to the new position. The length of the jump is vt. This is probably the most often used coupled continuous-time random walk model (see, e.g., [16, 18, 19, 26]).

- Jump-first model: the random walker first jumps instantaneously along the vector $\mathbf{r}$ and then waits in the new position for the time $t = |\mathbf{r}|/v$ (cf. [28]). This model can probably describe the motion of bacteria or animals that first move for a certain distance and then rest to recover for a time that depends on the length of the previous jump.

- Velocity model: the random walker moves within a step with constant velocity v from the old to the new position. To describe the behavior of most real systems, this model is more suitable than the previous ones because the instantaneous jumps that occur in the wait-first and jump-first model are usually unphysical. The velocity model corresponds to the Lévy Walk model (see [2, 21]).

In [22], the wait-first and the velocity model are studied and compared in detail.

The PDF $P(\mathbf{r}, t)$ for the standard CTRW and for the coupled models can be determined in Fourier–Laplace space by solving integral equations. We introduce the additional probability density $Q(\mathbf{r}, t)$ for the event that a step ends at a position between $\mathbf{r}$ and $\mathbf{r} + d\mathbf{r}$ in the time interval $[t, t + dt]$. In the standard CTRW model, we find the

following integral equation for $Q(\mathbf{r}, t)$ (see, e.g., [20]):

$$Q(\mathbf{r}, t) = \int_0^\infty \mathrm{d}t' \int \mathrm{d}\mathbf{r}' g_s(\mathbf{r}') f(t') Q(\mathbf{r} - \mathbf{r}', t - t') + \delta(\mathbf{r})\delta(t), \tag{7}$$

i.e. the probability $Q(\mathbf{r}, t)$ that a step ends at $\mathbf{r}$ at time t is given by integrating $Q(\mathbf{r} - \mathbf{r}', t - t')$ over all possible jumps $\mathbf{r}'$ and waiting times t'. Here $f(t')$ and $g_s(t')$ are given by the power law distributions (4) and (5). $Q(\mathbf{r} - \mathbf{r}', t - t')$ is the probability that the previous step ended in $\mathbf{r} - \mathbf{r}'$ at time $t - t'$. It then waited for time t' before it jumped to $\mathbf{r}$ along $\mathbf{r}'$. The term $\delta(\mathbf{r})\delta(t)$ in (7) is due to the initial conditions.

The corresponding integral equation for all coupled models is

$$Q(\mathbf{r}, t) = \int_0^\infty \mathrm{d}t' \int \mathrm{d}\mathbf{r}' \, f(t')\delta(t' - |\mathbf{r}'|/v) Q(\mathbf{r} - \mathbf{r}', t - t') + \delta(\mathbf{r})\delta(t). \tag{8}$$

The factor $\delta(t' - |\mathbf{r}'|/v)$ is due to the coupling of the step length and its duration. Further details are given in appendix A.

We can now calculate the PDF $P(\mathbf{r}, t)$ for the different models with the help of $Q(\mathbf{r}, t)$. For example, for the standard and the wait-first model denoted respectively by the indices s and w

$$P_{s,w}(\mathbf{r}, t) = \int_0^t \mathrm{d}t' \, Q(\mathbf{r}, t - t') F_{s,w}(t'), \tag{9}$$

where $F_{s,w}(t)$ is the probability that the random walker does not jump with certainty during the time interval t, i.e.

$$F_{s,w}(t) = 1 - \int_0^t \mathrm{d}t' \, f(t'). \tag{10}$$

In appendix A we also show how the PDF $P(\mathbf{r}, t)$ is calculated for the other models.

Note, for all coupled models, the steps start and end in the same points, they are only executed differently (see figure 1). As a consequence, $Q(\mathbf{r}, t)$ is also the same. Therefore, this formalism embraces all coupled models studied so far in the literature. On the one hand, it allows us to treat them in a unified way, while, on the other hand, it is also capable of including more complicated forms of coupling. Yet another positive feature is that the integral equations can be solved analytically.

By using the Fourier–Laplace transformation

$$\bar{P}(\mathbf{k}, s) = \mathcal{F}(\mathcal{L}(P(\mathbf{r}, t))) = \int \mathrm{d}\mathbf{r} \int_0^\infty \mathrm{d}t \, \mathrm{e}^{\mathrm{i}\mathbf{k}\cdot\mathbf{r}} \mathrm{e}^{-st} P(\mathbf{r}, t), \tag{11}$$

one finds the well-known result for the standard model (see appendix A for details or, for example, [17, 24])

$$\bar{P}_s(\mathbf{k}, s) = \frac{\bar{F}_s(s)}{1 - \bar{g}_s(\mathbf{k})\bar{f}(s)} \tag{12}$$

with $\bar{F}_s(s) = (1 - \bar{f}(s))/s$. $\tag{13}$

For the coupled models, the PDF in Fourier–Laplace space is (cf., e.g., [2, 16, 18, 19, 21, 22, 26, 28])

$$\bar{P}_{j,w,v}(\mathbf{k}, s) = \frac{\bar{F}_{j,w,v}(\mathbf{k}, s)}{1 - \mathcal{F}(\mathrm{e}^{-s|\mathbf{r}|/v}g(|\mathbf{r}|))}, \tag{14}$$

where $\bar{F}_{j,w,v}(\mathbf{k}, s)$ depends on the model and is given in appendix A.

The results in (12) and (14) are the exact solutions in Fourier–Laplace space. For the standard model the denominator in (12) contains the product $\bar{g}_s(\mathbf{k})$ times $\bar{f}(s)$. However, for the coupled models, the corresponding function in the denominator of (14) does not factorize. Although the numerator in (14) depends on the type of the model, the denominator in (14) is the same for all coupled models. We will show that this is the reason that the central part of the PDF has the same scaling behavior for all these models. Usually, the inverse Fourier–Laplace transformations of (12) and (14) cannot be calculated analytically. In the following sections we therefore use these equations as the starting point and show and discuss how different approximations can be employed to reveal their characterizing properties.

3. Scaling of the mean square displacement

The MSD is defined by

$$\langle r^2(t) \rangle = \int \mathrm{d}\mathbf{r} |\mathbf{r}|^2 P(\mathbf{r}, t). \tag{15}$$

In Laplace space this corresponds to

$$\langle r^2(s) \rangle = \mathcal{L}(\langle r^2(t) \rangle) = -\nabla_k^2 \bar{P}(\mathbf{k}, s)|_{\mathbf{k}=\mathbf{0}}. \tag{16}$$

Therefore, the MSD can be calculated using the expansion of $\bar{P}(\mathbf{k}, s)$ up to the second order in $\mathbf{k}$. Furthermore, the asymptotic long-time behavior of $\langle r^2(t) \rangle$ can be obtained by calculating the small s expansion of $\bar{P}(\mathbf{k}, s)$. As a consequence, usually $\bar{P}(\mathbf{k}, s)$ is evaluated by first considering the limit $|\mathbf{k}| \to 0$ and then expanding the result for small s.

For simplicity, in the following, we consider a random walk in one dimension. However, most of the results presented can be determined for a higher-dimensional space in a similar way. For the standard model, the expansion of the numerator in (12) then is

$$\bar{F}_s(s) \approx \Gamma(1 - \mu)s^{\mu-1} + \frac{1}{\mu - 1}. \tag{17}$$

Concentrating on only the lowest order term in s, one finds

$$\bar{F}_s(s) \approx \begin{cases} \Gamma(1 - \mu)s^{\mu-1}, & \mu < 1 \\ \dfrac{1}{\mu - 1}, & \mu > 1. \end{cases} \tag{18}$$

The denominator is

$$1 - \bar{g}_s(k)\bar{f}(s) \approx n_1(s) + n_2(k) \qquad \text{with } n_1(s) = \begin{cases} \Gamma(1-\mu)s^\mu, & \mu < 1 \\ \dfrac{1}{\mu-1}s, & \mu > 1 \end{cases}$$

$$\text{and } n_2(k) = \begin{cases} \dfrac{\pi}{2\sin(\pi\beta/2)\Gamma(\beta)}|k|^\beta, & \beta < 2 \\ \dfrac{1}{\beta^2 - 3\beta + 2}k^2, & \beta > 2. \end{cases} \tag{19}$$

Therefore, the PDF has the form

$$\bar{P}_s(k,s) \approx \begin{cases} \dfrac{s^{\mu-1}}{s^\mu + C|k|^\beta}, & \mu < 1, \quad \beta < 2 \\ \dfrac{s^{\mu-1}}{s^\mu + C'k^2}, & \mu < 1, \quad \beta > 2 \\ \dfrac{1}{s + C|k|^\beta}, & \mu > 1, \quad \beta < 2 \\ \dfrac{1}{s + C'k^2}, & \mu > 1, \quad \beta > 2, \end{cases} \tag{20}$$

where C, and C' are constants that only depend on β and μ. Note, for limiting cases like $\beta = 2$, there may be logarithmic corrections. However, we will not consider such cases in the following. Unlike the expansions for the coupled models that we will calculate later in this section, (20) does not depend on the order in which the limits $s \to 0$ and $k \to 0$ are considered and therefore can also be used for the considerations in the next section. For $\beta < 2$ the second moment of the step length distribution $\int_{-\infty}^{\infty} dx\, g(|x|)x^2$ is infinite and the MSD diverges. By using (16), one finds for $\beta > 2$

$$\langle r_s^2(s) \rangle \propto \begin{cases} s^{-\mu-1}, & \mu < 1 \\ s^{-2}, & \mu > 1. \end{cases} \tag{21}$$

Therefore, in the long-time limit (cf., e.g., [24])

$$\langle r_s^2(t) \rangle \propto \begin{cases} t^\mu, & \mu < 1 \\ t, & \mu > 1, \end{cases} \tag{22}$$

i.e. if $\beta > 2$ the system is subdiffusive for $\mu < 1$ and diffusive for $\mu > 1$.

For the coupled models the order in which the limits $s \to 0$ and $|\mathbf{k}| \to 0$ are performed usually matters. To determine the scaling of the MSD, first the limit of small k and then the limit $s \ll 1$ has to be considered. The calculations are similar to the ones for the standard model. The expansion in small k and small s for the numerator and the denominator of (14) are treated separately. The MSD is then determined by using (16). Details are given in appendix B.

For the jump-first model the MSD diverges for $\mu < 2$ because the second moment of the step length distribution is infinite. For $\mu > 2$ normal diffusion occurs.

Interestingly, the scaling of the MSD is the same for the wait-first model and for the velocity model. One finds (see, e.g., [20] for the wait-first and [18] for the velocity model)

$$\langle r_{w,v}^2(t)\rangle \propto \begin{cases} t^2, & \mu < 1 \\ t^{3-\mu}, & 1 < \mu < 2 \\ t, & \mu > 2, \end{cases} \tag{23}$$

i.e. the motion is ballistic for $\mu < 1$, superdiffusive for $1 < \mu < 2$ and normal diffusion occurs for $\mu > 2$. Obviously, the MSD does not provide sufficient information to distinguish the wait-first and the velocity model.

4. Scaling of the probability distribution function

In this section we discuss the scaling property of the PDF $P(x,t)$. We determine the exponent α defined in (2) for the central part of $P(x,t)$ where $x/t^\alpha \ll 1$. We first calculate expansions of the numerator and denominator of the PDF in Fourier–Laplace space as given by (12) or (14) with respect to $s \to 0$ corresponding to $t \to \infty$. Then we further expand the results with respect to $k \to 0$. The order in which the limits are considered guarantees $k \gg s^{\alpha+1}$ and therefore $x \ll t^\alpha$. As we will show later in this section, one finds

$$\bar{P}(k,s) \approx \frac{s^{\kappa_1} k^{\kappa_2}}{c_1 s^{\lambda_1} + c_2 k^{\lambda_2}} \tag{24}$$

where κ_1, κ_2, λ_1 and λ_2 depend on the model, on the step duration exponent μ, and, in the standard model, on the step length exponent β. Note that the exponents κ_1 and κ_2 are functions of λ_1 and λ_2 due to the normalization of $\bar{P}(k,s)$. Applying the inverse Fourier–Laplace transformations, one finds

$$P(x,t) \approx \frac{1}{4\pi^2 i} \int_{\epsilon-i\infty}^{\epsilon+i\infty} ds \int_{-\infty}^{\infty} dk \, e^{st-ikx} \frac{s^{\kappa_1} k^{\kappa_2}}{c_1 s^{\lambda_1} + c_2 k^{\lambda_2}}, \tag{25}$$

where ϵ is a real number chosen such that the path of integration is in the region of convergence. Using the substitutions $s' = st$ and $k' = kx$, (25) can be written in the form

$$P(x,t) \approx \frac{1}{t^{\lambda_1/\lambda_2}} \Phi\left(\frac{x}{t^{\lambda_1/\lambda_2}}\right). \tag{26}$$

By comparing (26) and (2), one finds $\alpha = \lambda_1/\lambda_2$ (cf., e.g., [20], [25]–[27]), i.e. the scaling exponent α is given by the exponents in the expansion of the denominator of $\bar{P}(k,s)$.

In the standard model the order in which the limits $k \to 0$ and $s \to 0$ are considered does not matter. Therefore the PDF is given by (20) and one finds the scaling exponent (cf., e.g., [24])

$$\alpha = \begin{cases} \mu/\beta, & \mu < 1, \quad \beta < 2 \\ 1/\beta, & \mu > 1, \quad \beta < 2 \\ \mu/2, & \mu < 1, \quad \beta > 2 \\ 1/2, & \mu > 1, \quad \beta > 2. \end{cases} \tag{27}$$

For the coupled models the order of the limits $k \to 0$ and $s \to 0$ does not commute and as a consequence, as we will show in the following, the scaling of the central part of $P(x,t)$ differs from the scaling of the MSD. Expanding first with respect to $s \ll 1$ and then with respect to $k \ll 1$, the denominator of $\bar{P}(k,s)$ for the coupled models in one dimension is

$$1 - \mathcal{F}(e^{-s|x|/v}g(|x|)) \approx \begin{cases} C_1 s k^{\mu-1} + C_2 k^{\mu}, & \mu < 1 \\ C_1' s + C_2 k^{\mu}, & 1 < \mu < 2 \\ C_1' s + C_2' k^2, & \mu > 2. \end{cases} \tag{28}$$

Therefore, one finds

$$\alpha = \begin{cases} 1, & \mu < 1 \\ 1/\mu, & 1 < \mu < 2 \\ 1/2, & \mu > 2. \end{cases} \tag{29}$$

Note, if the step length and the waiting time distribution in the standard model have the same exponent, i.e. if $\beta = \mu$, the scaling exponent for the standard model in (27) equals the scaling exponent of the coupled models in (29).

Note that the wait-first and the velocity model exhibit superdiffusion for $1 < \mu < 2$ because the exponent ν according to (23) gives $(3 - \mu)/2$. On the other hand, according to (29) $\alpha = 1/\mu \neq \nu$.

In figure 2 we plot the rescaled PDF $P(r,t)$ for the velocity model with $\mu = 1.5$ obtained by a simulation with 10 000 runs. In figure 2(a) $P(r,t)$ is rescaled using the exponent $\alpha = 2/3$ given by (29). For comparison, in figure 2(b) we have employed the exponent ν defined in (1) which according to (23) is $\nu = 3/4$. Figure 2 shows that the exponent determined by the MSD does not lead to the correct scaling behavior of $P(r,t)$; especially close to $x = 0$ the PDFs rescaled with ν do not collapse on a unique curve. However, the rescaling with the exponent α works very well. There are only minor deviations in the tails (not shown in figure 2), because the PDF does not scale perfectly. From simulations, we obtain similar results for the wait-first model and α also correctly describes the scaling of the jump-first model, where the MSD does not exist at all. Therefore, for the coupled models the scaling property of the PDF is not given by the exponent ν obtained from the MSD, but by α as determined in (29), which for $1 < \mu < 2$ differs from ν.

5. Profile of the probability distribution function

The methods presented in the previous sections allow us to only determine the central part of the PDF with $x \ll t^{\alpha}$ and the MSD. In order to obtain the profile of the PDF in the region where x is of the order of t^{α}, a different way to calculate the limits $s \to 0$ and $k \to 0$ has to be employed. In this section we introduce a method how to calculate the limits $s \to 0$ and $k \to 0$ simultaneously. This method leads to a very good approximation of the PDF and also to the correct scaling. However, it usually is technically more difficult than the methods presented so far.
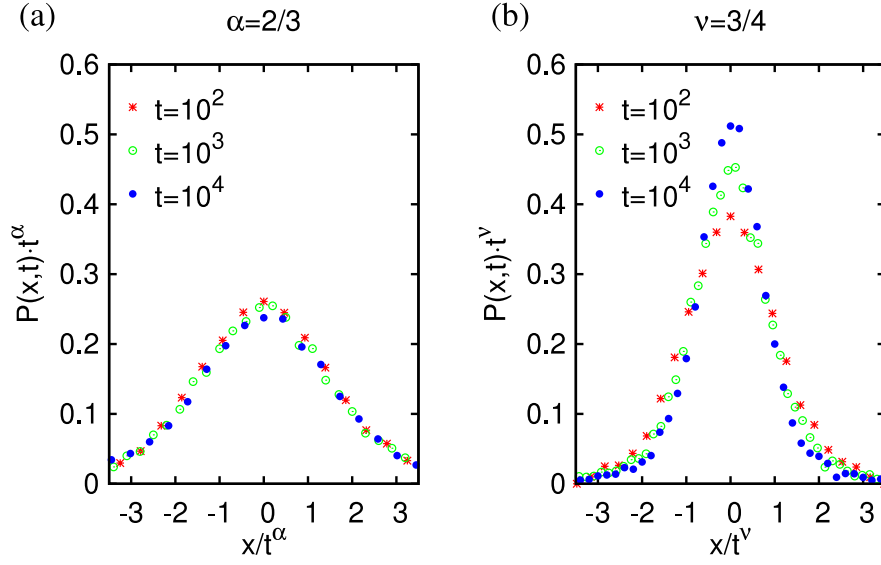
Figure 2. Rescaled PDF for the velocity model with $\mu = 1.5$. In (a) the exponent $\alpha = 2/3$ as determined by (29) is employed for the rescaling; in (b) the exponent of the MSD $\nu = 3/4$ (cf. (23)) is used.

The denominator of $\bar{P}(\mathbf{k}, s)$ for the coupled models is

$$
\begin{aligned}
1 - \mathcal{F}(\mathrm{e}^{-s|x|/v} g(|x|)) &= 1 - \int_{-\infty}^{0} \mathrm{d}x\, \mathrm{e}^{\mathrm{i}kx}\, \mathrm{e}^{sx/v} g(-x) + \int_{0}^{\infty} \mathrm{d}x\, \mathrm{e}^{\mathrm{i}kx}\, \mathrm{e}^{-sx/v} g(x) \\
&= 1 - \int_{0}^{\infty} \mathrm{d}x\, \mathrm{e}^{-\mathrm{i}kx - sx/v} g(x) + \int_{0}^{\infty} \mathrm{d}x\, \mathrm{e}^{\mathrm{i}kx - sx/v} g(x) \\
&= 1 - h(-k + \mathrm{i}s/v) + h(k + \mathrm{i}s/v)
\end{aligned}
\tag{30}
$$

with $h(z) = \mathcal{F}(g(x)\theta(x))|_{k=z}$, where $\theta(x)$ is the Heaviside step function. The denominator only depends on $-k + \mathrm{i}s/v$ and $k + \mathrm{i}s/v$ and the limit $s, k \to 0$ can be determined by using the expansion of $h(z)$ for small z. Expansions of the form (30) and their connection to solutions of fractional diffusion equations were studied, for example, in [25]–[27]. Using (6) and (4), one finds

$$
1 - \mathcal{F}(\mathrm{e}^{-s|x|/v} g(|x|)) \approx c_1 s + c_2 k^2 + c_3 s^2 + c_4 (\mathrm{i}s/v + k)^\mu + c_4 (\mathrm{i}s/v - k)^\mu.
\tag{31}
$$

This leads to the scaling behavior of the PDF that has already been determined in the previous section (cf. (29)). Furthermore, an inverse Fourier–Laplace transformation gives an excellent approximation of the PDF (see figure 3). However, since by taking $k \to 0$ and $s \to 0$ simultaneously, the tails of the PDF (in this example this means locations in the vicinity of the light front $x = vt$) usually are not obtained correctly. In general, it is therefore not possible to determine the correct exponent of the MSD from (31). Hence, the method presented in this section cannot replace the one presented in section 3 that allows us to determine the MSD as a function of time.

In figure 3 we show that the three different ways to calculate limits of $\bar{P}_w(k, s)$ lead to different PDFs in real space. The PDFs are obtained for the wait-first model with $\mu = 1/2$. The stars denote the simulation result. If first the limit $k \to 0$ and then $s \to 0$ is

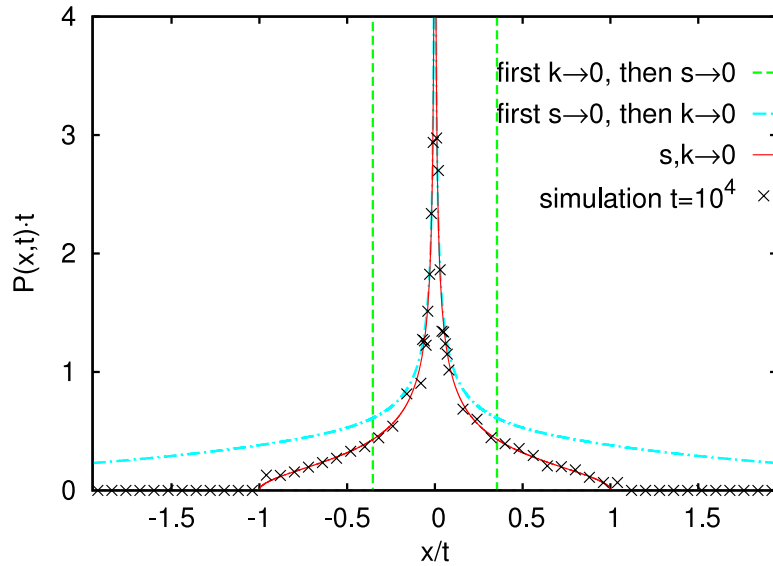**Figure 3.** PDF obtained from different limits of $\bar{P}_w(k,s)$ for the wait-first model with $\mu = 1/2$. The dashed lines denote two δ peaks that result from first considering $k \to 0$ and then $s \to 0$ and is used to calculate the MSD as described in section 3 and in appendix B. The dashed–dotted line is determined by first calculating $s \to 0$ and then $k \to 0$ and correctly describes the scaling of the central part of the PDF as shown in section 4. The solid line is achieved by considering $s \to 0$ and $k \to 0$ simultaneously and gives the correct asymptotic behavior of the PDF (cf. section 5). The crosses denote the result of a simulation with 10 000 runs.

considered (see (B.5) in the appendix), the inverse Fourier–Laplace transformation leads to two δ peaks (dashed lines in figure 3) that correctly mark the MSD but differ from the correct PDF. By first calculating $s \to 0$ and then $k \to 0$ (cf. (28)), only the correct behavior of the central part of the PDF is obtained (dashed–dotted line). The profile of the PDF determined by considering $s, k \to 0$ simultaneously (cf. (31)) leads to a much better representation of the PDF (solid line).

6. Scaling of moments

Finally, we consider the scaling of different moments of the PDF. In figure 4 the exponent $q\nu(q)$ defined by $\langle|\mathbf{r}(t)|^q\rangle \propto t^{q\nu(q)}$ is shown as a function of q for the velocity model and different exponents μ. This kind of analysis of the moments is known for many systems, e.g. for billiard models [6]–[8] or other systems that exhibit anomalous diffusion [12, 31, 32]. Systems with non-constant $\nu(q)$ are sometimes called strongly anomalous diffusive (cf. [31]). In particular, in many systems one finds a crossover from a linear behavior for small q to a second linear regime for large q. The velocity model (see figure 4) and the wait-first model are examples for such a behavior. We find that the slope for small q, i.e. $\lim_{q\to 0}\nu(q)$ equals the scaling exponent α of the probability distribution function $P(r,t)$ (see figure 5). This is reasonable, because small moments are mainly determined by the central part of $P(r,t)$, which scales with the exponent α.
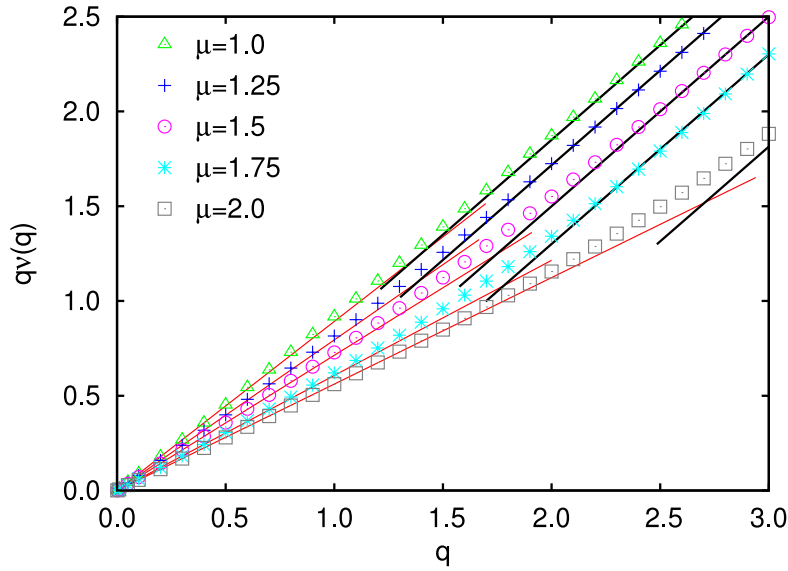
Figure 4. Scaling exponent $q\nu(q)$ for the qth moment of the PDF as a function of q for the velocity model and different exponents μ. The lines are fits to the behavior of the moments for small or large q, respectively.

For large q, the slope of $q\nu(q)$ becomes approximately 1, which is in agreement with the findings in [6]–[8], [31] and is due to the outermost particles that travel ballistically with the velocity v given by the coupling and dominate the higher moments. For the jump-first model we also find $\alpha = \lim_{q \to 0} \nu(q)$ but higher moments do not exist. In figure 5 we plot the scaling exponents of the MSD and of the PDF as a function of μ. Results of simulations (points) are in good agreement with theoretical predictions (lines).

7. Analyzing data of experiments or simulations

We have shown that the exponent in the power law of the MSD is not sufficient for characterizing the full scaling properties of many systems exhibiting anomalous diffusion. Therefore, a careful analysis of experimental data should at least contain the fractional scaling exponents as introduced in the previous section. Using positional data of particles at different times, first the time dependence of the qth moments $\langle |\mathbf{r}(t)|^q \rangle = \langle |\mathbf{r}(t) - \mathbf{r}(0)|^q \rangle$ is calculated and then by fitting it to the power law $\langle |\mathbf{r}(t)|^q \rangle \propto t^{q\nu(q)}$ the fractional scaling exponent $q\nu(q)$ is obtained. This method was already employed to analyze some billiard models [6]–[8] as well as anomalous diffusion generated by maps [31]. In this section we will show that this relatively simple method of analysis has a significantly broader predictive and explanatory power and is not limited to the concrete examples considered before. We introduce another model to generate numerical data that we analyze for illustration. Consider a system of Langevin equations that was suggested as a continuum analog of a Lévy walk process [33] (note that it is one of three commonly used models [35]–[37]). It consists of the following three equations:

$$\frac{\mathrm{d}x}{\mathrm{d}t} = v(t) \qquad \frac{\mathrm{d}v}{\mathrm{d}s} = -\gamma v(s) + \xi(s) \qquad \frac{\mathrm{d}t}{\mathrm{d}s} = \eta_\mu(s). \tag{32}$$
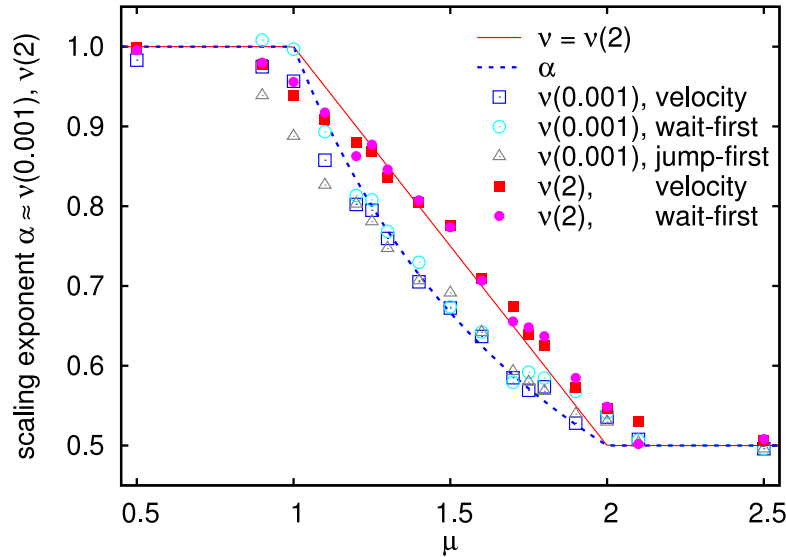
Figure 5. Exponents $\nu = \nu(2)$ (solid symbols) and $\alpha \approx \lim_{q\to 0} \nu(q)$ (open symbols) describing respectively the scaling of the MSD and of the PDF as a function of μ for the coupled models. For simplicity, we take $\lim_{q\to 0} \nu(q) \approx \nu(0.001)$. The points are obtained from simulations averaged over $10\,000$ runs by analyzing the moments with $q = 0.001$ and $q = 2$; the lines represent the theoretical predictions given in (23) and (29).

The first equation is just the definition of velocity as a function of time t. The second equation is a standard Langevin equation with a Gaussian delta correlated white noise $\xi(s)$, but with velocity being a function of an internal time s. The last equation describes the evolution of the physical time t as a stochastic process in the internal time s (note that this description is also called subordination). Here η represents Lévy noise with realizations taken from a Lévy distribution characterized asymptotically by a power law decay with exponent $1 + \mu$, where $0 < \mu \leq 2$. On a qualitative level this system can be understood as follows. The second equation leads to a Gaussian distribution of velocities and the third equation gives a distribution of flight times with an asymptotic behavior according to a power law. For $0 < \mu < 1$, the mean flight time is infinite and we are in the situation of Lévy walks with ballistic scaling. However, for $1 < \mu < 2$, the random walks will be superdiffusive with scaling properties highlighted in this paper. To be more precise, such a system of Langevin equations is equivalent to the model of random walks with random velocities where velocities and flight times are drawn from Gaussian and power law distributions, respectively [23, 30].

Our goal now is to produce trajectories governed by (32) and analyze their statistical properties. For the details on an efficient algorithm for generating such trajectories, we refer to [34] and for general methods of numerical solutions of stochastic differential equations to a comprehensive book [38]. For our simulations we choose $\mu = 1.4$ and set all other constants to be equal to 1.0. We have simulated 10^5 trajectories of a maximal length 10^5. The resulting exponents $\nu(q)$ are illustrated in figure 6 and show the typical and familiar behavior described above. The exponents $q\nu(q)$ for $q \gg 1$ reveal the scaling
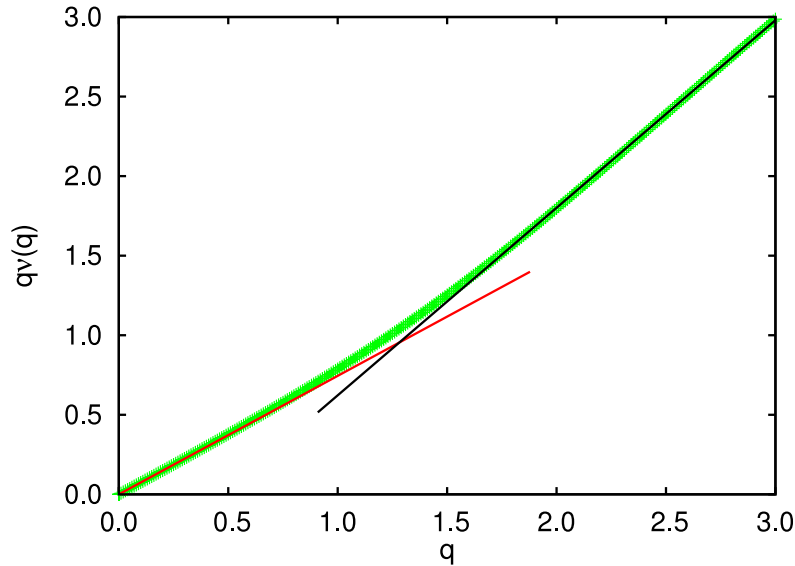
Figure 6. Scaling exponent $q\nu(q)$ for the qth moment of the PDF as a function of q for the simulation data obtained by the modified Langevin formalism described in the text. The lines are fits to the data for small or large q.

of the tails of the PDF which is dominated by the velocity of the random walker. For $q \ll 1$, $\nu(q)$ approaches the scaling exponent α that determines the scaling of the central part of the PDF. In our specific example, we identify the scaling exponent of the mean squared displacement $\nu(2) \simeq 0.79$ (the theoretically expected value is $(1 - \mu)/2 = 0.8$) and the scaling exponent of the central part of the PDF given by the moments for small q values, $\nu(q) \simeq 0.74$ (expected value $1/\mu \simeq 0.71$).

So far a relatively large number of trajectories was used in our examples in order to produce smooth curves like the one shown in figure 6. However, in real experiments such large numbers are usually unattainable (see, e.g., [4, 10, 14]). Therefore, in our last example, we analyze data of simulations of the wait-first model averaged over only thirty trajectories. In figure 7 we plot the fourth root of the fourth moment, the square root of the MSD and the tenth power of the moment with exponent 0.1. The lines indicate the asymptotic behavior for the MSD and the moment with exponent 0.1. Interestingly, the data showing the time dependence of the moment with exponent 0.1 reaches the asymptotic behavior at large times. On the other hand, the data displaying the MSD and especially those showing the fourth moment possess a lot of jumps. For the fourth moment it is even impossible to determine a proper asymptotic fit to the given data. Therefore, to find the correct asymptotic behavior, only a small number or long trajectories is needed if moments with small exponents are considered. To properly analyze the MSD or higher moments, a larger number of runs is necessary.

In conclusion, characterizing the scaling behavior of an experimental system, the moments with small exponents reveal directly the scaling of the central part of the PDF. The scaling exponent of the MSD is usually more difficult to obtain and may differ from the scaling exponent of the PDF.
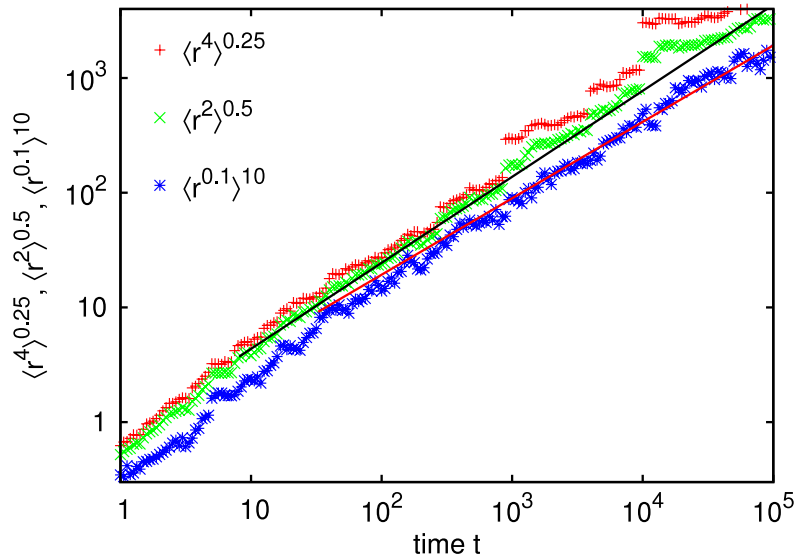
Figure 7. Fourth root of the fourth moment, square root of the mean square displacement and tenth power of the moment with exponent 0.1 averaged over 30 trajectories obtained by a simulation of the wait-first model with $\mu = 1.5$. The lines indicate the asymptotic behavior. For the fourth moment the asymptotic behavior cannot be properly determined due to the large jumps.

Table 1. Overview of scaling properties of a random walk that follow from various limiting cases. A cross denotes that the corresponding exponent or function can be obtained by calculating the limits $k \to 0$ and $s \to 0$ in the indicated order or by analyzing the fractional moments. The exponent α characterizes the scaling of the central part of the PDF, ν is the exponent given by the MSD and Φ is the rescaled PDF as introduced in (2).

	α	ν	Φ
First $k \to 0$, then $s \to 0$		$\times$	
First $s \to 0$, then $k \to 0$	$\times$		
$s, k \to 0$ simultaneously	$\times$		$\times$
Fractional moments	$\times$	$\times$	

8. Conclusions

Based on a universal description developed for coupled random walks, we have presented three different methods for calculating exponents that characterize anomalous diffusion (see table 1). The exponent $\nu = \nu(2)$ defined by the mean square displacement as a function of time is determined by first considering the limit $k \to 0$ and then $s \to 0$ in the Fourier–Laplace representation of the PDF. However, especially in the superdiffusive regime, ν may differ from the exponent α that describes the scaling of the central part of the PDF and is obtained by reversing the order in which the limits $s \to 0$ and $k \to 0$ are calculated. In order to find an optimal representation of the PDF, the limits $s \to 0$ and $k \to 0$ should be determined simultaneously. Note, the three methods of considering the limit $s, k \to 0$ are all clearly distinct from each other. Each of the three methods

only reveals some dynamic properties while it cannot substitute the other methods to completely analyze the system.

We also evaluate the exponents $\nu(q)$ defined by the fractional moments $\langle|\mathbf{r}|^q\rangle$ and found a transition from a regime with $\nu(q) \approx \alpha$ for small q to a regime where $q\nu(q)$ has slope 1 for large q. This result is important for analyzing data obtained in experiments or by simulations. While the analysis of the mean square displacement may not lead to the correct scaling exponent α, moments $\langle|\mathbf{r}|^q\rangle$ with small q reveal the right scaling behavior because $\alpha = \lim_{q\to 0} \nu(q)$.

Acknowledgments

Appendix A. Calculation of the probability distribution function in Fourier–Laplace space

In the following, we determine the PDF $P(\mathbf{r}, t)$ for the standard CTRW and for the coupled models by introducing integral equations, which are then solved in Fourier–Laplace space.

We employ the probability density $Q(\mathbf{r}, t)$ for the event that a step ends as introduced in the main text and find (7) for the standard CTRW model. For all coupled models, (8) is the integral equation for $Q(\mathbf{r}, t)$. Integrating over time and using (6) and (8) becomes

$$Q(\mathbf{r}, t) = \int_{|\mathbf{r}'|\leq vt} \mathrm{d}\mathbf{r}' g(|\mathbf{r}'|) Q(\mathbf{r} - \mathbf{r}', t - |\mathbf{r}'|/v) + \delta(\mathbf{r})\delta(t), \qquad (A.1)$$

i.e. a step ends at time t at position $\mathbf{r}$ if the previous step has ended in $\mathbf{r} - \mathbf{r}'$ at time $t - |\mathbf{r}'|/v$. The vector $\mathbf{r}'$ describes the change of position during a step and occurs with probability $g(|\mathbf{r}'|)$ and only steps with length $|\mathbf{r}'| \leq vt$ are allowed since the walker starts at $t = 0$ at $\mathbf{r} = \mathbf{0}$.

The PDF $P(\mathbf{r}, t)$ for the different models can be calculated with the help of $Q(\mathbf{r}, t)$. For the standard and the wait-first model we find (9) as already explained in the main text. For the jump-first model

$$P_j(\mathbf{r}, t) = \int \mathrm{d}\mathbf{r}' \int_0^{|\mathbf{r}'|/v} \mathrm{d}t' \, g(|\mathbf{r}'|) Q(\mathbf{r} - \mathbf{r}', t - t'). \qquad (A.2)$$

The velocity model leads to

$$P_v(\mathbf{r}, t) = \int_{|\mathbf{r}'|\leq vt} \mathrm{d}\mathbf{r}' \, Q(\mathbf{r} - \mathbf{r}', t - |\mathbf{r}'|/v) G(|\mathbf{r}'|) \qquad (A.3)$$

where $G(|\mathbf{r}|)$ is the probability that the step length is larger than $|\mathbf{r}|$, i.e.

$$G_v(|\mathbf{r}|) = 1 - \int_{|\mathbf{r}'|<|\mathbf{r}|} \mathrm{d}\mathbf{r}' \, g(|\mathbf{r}'|). \qquad (A.4)$$

This closes the set of integral equations for $Q(\mathbf{r}, t)$ and $P(\mathbf{r}, t)$.

To solve all these integral equations, we apply the Fourier–Laplace transformation as given in (11). Due to the convolution property of the Fourier–Laplace transformation, (9), (A.2) and (A.3) assume the form

$$\bar{P}(\mathbf{k}, s) = \bar{Q}(\mathbf{k}, s)\bar{F}(\mathbf{k}, s), \tag{A.5}$$

where $\bar{P}(\mathbf{k}, s)$ stands for $\bar{P}_s(\mathbf{k}, s)$, $\bar{P}_w(\mathbf{k}, s)$, $\bar{P}_j(\mathbf{k}, s)$ or $\bar{P}_v(\mathbf{k}, s)$ and $\bar{F}(\mathbf{k}, s)$ represents the following convoluted functions in Laplace or Fourier–Laplace space:

$$\bar{F}_{s,w}(s) = \mathcal{L}(F_{s,w}(t)) = (1 - \bar{f}(s))/s, \tag{A.6}$$

$$\bar{F}_j(\mathbf{k}, s) = \mathcal{F}(g(|\mathbf{r}|)[1 - \mathrm{e}^{-s|\mathbf{r}|/v}]/s), \tag{A.7}$$

$$\text{or } \bar{F}_v(\mathbf{k}, s) = \mathcal{F}(\mathrm{e}^{-s|\mathbf{r}|/v}G(|\mathbf{r}|)). \tag{A.8}$$

In order to obtain (A.7) and (A.8), the time-shifting property of the Laplace transformation was employed, which leads to the factors $\mathrm{e}^{-s|\mathbf{r}|/v}$ in Laplace space because the original function was displaced by $-|\mathbf{r}|/v$.

For the standard model, (7) in Fourier–Laplace space becomes

$$\bar{Q}(\mathbf{k}, s) = \bar{g}_s(\mathbf{k})\bar{f}(s)\bar{Q}(\mathbf{k}, s) + 1. \tag{A.9}$$

Combining (A.5) and (A.9), one finds the well-known result (12).

For the coupled models, using (A.1) in Fourier–Laplace space, i.e.

$$\bar{Q}(\mathbf{k}, s) = \bar{Q}(\mathbf{k}, s)\mathcal{F}(\mathrm{e}^{-s|\mathbf{r}|/v}g(|\mathbf{r}|)) + 1, \tag{A.10}$$

one obtains the exact solution (14) of the PDF in Fourier–Laplace space, where the numerator is

$$\bar{F}_w(s) = (1 - \bar{f}(s))/s \qquad \text{for the wait-first model}, \tag{A.11}$$

$$\bar{F}_j(\mathbf{k}, s) = \mathcal{F}(g(|\mathbf{r}|)[1 - \mathrm{e}^{-s|\mathbf{r}|/v}]/s) \qquad \text{for the jump-first model}, \tag{A.12}$$

$$\text{and } \bar{F}_v(\mathbf{k}, s) = \mathcal{F}(\mathrm{e}^{-s|\mathbf{r}|/v}G(|\mathbf{r}|)) \qquad \text{for the velocity model}. \tag{A.13}$$

Appendix B. Calculation of the scaling of the mean square displacement for the coupled models

Considering a one-dimensional random walk and first calculating the small k and then the small s expansions, we find for the denominator of (14) using (4) and (6)

$$1 - \mathcal{F}(\mathrm{e}^{-s|x|/v}g(|x|)) \approx \begin{cases} C_1 s^\mu + C_2 k^2 s^{\mu-2}, & \mu < 1 \\ C_1' s + C_2 k^2 s^{\mu-2}, & 1 < \mu < 2 \\ C_1' s + C_2' k^2, & \mu > 2, \end{cases} \tag{B.1}$$

where C_1, C_2, C_1' and C_2' are constants, only depending on μ and v. The numerator of (14) in the wait-first model is

$$\bar{F}_w(s) \approx \begin{cases} C_w' s^{\mu-1}, & \mu < 1 \\ C_w, & \mu > 1, \end{cases} \tag{B.2}$$

in the jump-first model

$$\bar{F}_j(s) \approx \begin{cases} C_{j,1}s^{-1} - C_{j,2}k^\mu s^{-1}, & \mu < 1 \\ C_{j,1}s^{-1} - C'_{j,2}ks^{-1}, & \mu > 1 \end{cases} \tag{B.3}$$

and in the velocity model

$$\bar{F}_v(k,s) \approx \begin{cases} C_{v,1}s^{\mu-1} - C_{v,2}k^2 s^{\mu-3}, & \mu < 1 \\ C'_{v,1} - C_{v,2}k^2 s^{\mu-3}, & \mu > 1. \end{cases} \tag{B.4}$$

Evaluating (14), we therefore find for the wait-first model

$$\bar{P}_w(k,s) \approx \begin{cases} \dfrac{C_w s}{C_1 s^2 + C'_2 k^2}, & \mu < 1 \\[2mm] \dfrac{C'_w}{C'_1 s + C'_2 k^2 s^{\mu-2}}, & 1 < \mu < 2 \\[2mm] \dfrac{C'_w}{C'_1 s + C_2 k^2}, & \mu > 2 \end{cases} \tag{B.5}$$

and calculate the MSD in Laplace space from (16)

$$\langle r_w^2(s) \rangle \propto \begin{cases} s^{-3}, & \mu < 1 \\ s^{\mu-4}, & 1 < \mu < 2 \\ s^{-2}, & \mu > 2. \end{cases} \tag{B.6}$$

Therefore, for real times in the long-time limit this becomes (23). A similar calculation for the velocity model also leads to (23), whereas the MSD of the jump-first model diverges for $\mu > 2$.

References

[1] Sancho J M, Lacasta A M, Lindenberg K, Sokolov I M and Romero A H, 2004 *Phys. Rev. Lett.* **92** 250601
[2] Shlesinger M F, West B J and Klafter J, 1987 *Phys. Rev. Lett.* **58** 1100
[3] Shlesinger M F, Zaslavsky G M and Klafter J, 1993 *Nature* **363** 31
[4] Solomon T H, Weeks E R and Swinney H L, 1993 *Phys. Rev. Lett.* **71** 3975
[5] Zacherl A, Geisel T, Nierwetberg J and Radons G, 1986 *Phys. Lett.* A **114** 317
[6] Armstead D N, Hunt B R and Ott E, 2003 *Phys. Rev.* E **67** 021110
[7] Sanders D P and Larralde H, 2006 *Phys. Rev.* E **73** 026205
[8] Schmiedeberg M and Stark H, 2006 *Phys. Rev.* E **73** 031113
[9] Schmitt F G and Seuront L, 2001 *Physica* A **301** 375
[10] Ramos-Fernández G, Mateos J L, Miramontes O, Cocho G, Larralde H and Ayala-Orozco B, 2004 *Behav. Ecol. Sociob.* **55** 223
[11] Upadhyaya A, Rieu J-P, Glazier J A and Sawada Y, 2004 *Physica* A **293** 549
[12] Reynolds A M and Frye M A, 2007 *PLOS One* **2** e354
[13] Dietrich P, Klages R, Preuss R and Schwab A, 2008 *Proc. Nat. Acad. Sci.* **105** 459
[14] Brockmann D, Hufnagel L and Geisel T, 2006 *Nature* **439** 462
[15] Gonzales M C, Midalgo C A and Barbasi A-L, 2008 *Nature* **453** 779
[16] Shlesinger M F, Klafter J and Wong Y M, 1982 *J. Stat. Phys.* **27** 499
[17] Montroll E W and Shlesinger M F, 1984 *Nonequilibrium Phenomena II: From Stochastic to Hydrodynamics* (*Studies in Statistical Mechanics* vol 11) ed J Leiboeitz and E W Montroll (Amsterdam: North-Holland) p 1
[18] Geisel T, Nierwetberg J and Zacherl A, 1985 *Phys. Rev. Lett.* **54** 616
[19] Shlesinger M F and Klafter J, 1985 *Phys. Rev. Lett.* **54** 2551

[20] Klafter J, Blumen A and Shlesinger M F, 1987 *Phys. Rev.* A **35** 3081
[21] Blumen A, Zumofen G and Klafter J, 1989 *Phys. Rev.* A **40** 3964
[22] Zumofen G and Klafter J, 1993 *Phys. Rev.* E **47** 851
[23] Klafter J and Barkai E, 1998 *Chaos, Kinetics and Nonlinear Dynamics in Fluids and Plasmas* (*Lecture Notes in Physics* vol 511) ed S Benkadda and G M Zaslavsky (Berlin: Springer) p 373
[24] Metzler R and Klafter J, 2000 *Phys. Rep.* **339** 1
[25] Barkai E, 2002 *Chem. Phys.* **284** 13
[26] Meerschaert M M, Benson D A, Scheffler H-P and Becker-Kern P, 2002 *Phys. Rev.* E **66** 060102R
[27] Zaburdaev V Yu and Chukbar K V, 2002 *J. Exp. Theor. Phys.* **94** 871
[28] Zaburdaev V Yu, 2006 *J. Stat. Phys.* **12** 871
[29] Friedrich R, Jenko F, Baule A and Eule S, 2006 *Phys. Rev. Lett.* **96** 230601
[30] Zaburdaev V Yu, Schmiedeberg M and Stark H, 2008 *Phys. Rev.* E **79** 011119
[31] Castiglione P, Mazzino A, Muratore-Ginanneschi P and Vulpiani A, 1999 *Physica* D **134** 75
[32] Chechkin A V and Gonchar V Yu, 2000 *Chaos, Solitons Fractals* **11** 2379
[33] Fogedby H C, 1994 *Phys. Rev.* E **50** 1657
[34] Kleinhans D and Friedrich R, 2007 *Phys. Rev.* E **76** 061102
[35] Eule S, Friedrich R, Jenko F and Kleinhans D, 2008 *J. Phys. Chem.* B **111** 11474
[36] Metzler R and Klafter J, 2000 *J. Phys. Chem.* B **104** 3851
[37] Barkai E and Silbey R, 2000 *J. Phys. Chem.* B **104** 3866
[38] Klöden P E and Platen E, 1992 *Applications of Mathematics* vol 23 *Numerical Solution of Stochastic Differential Equations* (Berlin: Springer)